Atmos. Chem. Phys. Discuss., 9, 4567–4607, 2009
www.atmos-chem-phys-discuss.net/9/4567/2009/

Atmospheric Chemistry and Physics Discussions

This discussion paper is/has been under review for the journal *Atmospheric Chemistry and Physics (ACP)*. Please refer to the corresponding final paper in *ACP* if available.

Oxygenated organic functional groups and their sources in single and submicron organic particles in MILAGRO 2006 campaign

S. Liu[1], S. Takahama[1], L. M. Russell[1], S. Gilardoni[1,2], and D. Baumgardner[3]

[1]Scripps Institution of Oceanography, Univ. of California, San Diego, La Jolla, California, USA
[2]Joint Research Centre, European Commission, Ispra, Italy
[3]Centro de Ciencias de la Atmósfera, Univ. Nacional Autónoma de México, México City, México

Received: 15 December 2008 – Accepted: 19 December 2008 – Published: 23 February 2009

Correspondence to: L. M. Russell (lmrussell@ucsd.edu)

Published by Copernicus Publications on behalf of the European Geosciences Union.

Abstract

Fourier Transform Infrared (FTIR) and X-ray Fluorescence (XRF) were used to measure organic functional groups and elements of submicron particles collected during MILAGRO in March 2006 on three platforms: the Mexico City urban area (SIMAT), the high altitude site at 4010 m (Altzomoni), and the NCAR C130 aircraft. Scanning transmission X-ray Microscopy (STXM) and Near-Edge X-ray Absorption Fine Structure (NEXAFS) were applied to single particle organic functional group abundance analysis of particles simultaneously collected at SIMAT and C130. Correlations of elemental concentrations showed different groups of source related elements at SIMAT, Altzomoni, and C130, suggesting different processes affecting the air masses sampled at the three platforms. Cluster analysis resulted in seven distinct Clusters of FTIR spectra, with the last three clusters consisting of spectra collected almost exclusively on the C130 platform, reflecting the variety of sources contributing to C130 samples. Positive Matrix Factorization (PMF) of NEXAFS-STXM spectra identified three main factors representing soot, secondary, and biomass burning type spectra. PMF of FTIR spectra resulted in three fossil fuel combustion type factors, one biomass burning factor, and one mixed or processed factor. The fossil fuel combustion type factors were found to have the largest contributions to OM, while the processed factor has the largest O/C among all factors. Alkane, carboxylic acid, and amine functional groups were mainly associated with combustion related sources, while alcohol groups were likely from atmospheric processing of mixed sources. While the processed factor has the highest O/C, half of the OM and O/C measured could be attributed directly to fossil fuel combustion sources. Both PMF of NEXAFS-STXM spectra and PMF of FTIR spectra indicate that the combustion type factors are more affected by fluctuations in local sources, while the processed factors are more consistent during the sampling period.

1 Introduction

Atmospheric aerosols have been causing more and more concerns during the last few decades since they reduce air quality (Eidels-Dubovoi, 2002), threaten human health (Dockery et al., 1993), and affect climate (Liepert et al., 2004). The effects of organic aerosols remain largely unknown because their compositions are complicated, especially in urban areas. Mexico City Metropolitan Area (MCMA) is the second largest megacity in the world. Although its pollution problem has been studied for more than 40 years (Raga et al., 2001), there are only a limited number of organic aerosol measurements (Salcedo et al., 2006; DeCarlo et al., 2008; Aiken et al., 2008, 2009). The main sources of MCMA include biomass burning (Johnson et al., 2006; Salcedo et al., 2006; Molina et al., 2007), motor vehicle emissions, oil burning, and crustal components (Querol et al., 2008; Stone et al., 2008).

The MILAGRO (Megacity Initiative: Local and Global Research Observations) campaign is the largest intensive measurement to date in MCMA to quantify properties of atmospheric aerosols. This study builds on the measurements presented by Gilardoni et al. (2009) to identify overall statistical trends that span the organic aerosol properties across the MCMA basin. Site-by-site correlations, clusters of organic types, and underlying source-related factors are combined in this work to identify the contributions to organic mass directly from the major source types in the MCMA and those formed later by atmospheric processing, possibly with contributions from multiple sources. In this work we also establish that the same organic functional group signatures and source types found in bulk submicron samples are evident in external mixtures of internally-mixed single particles.

Gilardoni et al. (2009) shows that the OM measurements from FTIR are well correlated with simultaneous AMS measurements during this campaign. Alkane functional groups dominated the OM. The average OM/OC and carboxylic acid COOH to aliphatic saturated C-C-H ratios were higher at Altzomoni than at SIMAT, as a consequence of a larger contribution of oxidized functional groups. The OM was found to correlate with

ACPD
9, 4567–4607, 2009

non-soil K, indicating biomass burning being a source of OM in MCMA.

In this paper, we will extend their work using chemometric techniques and specific statistical tests to identify additional and significant trends in the data set, in particular for normalized organic functional group composition and fraction of oxidized organic carbon. Correlations of each pair of elements and organic functional groups were investigated. The co-varying of organic functional groups with elemental markers provides an indication of the fraction of organic compound associated with specific metal source signatures. A Ward-type clustering technique was applied to FTIR spectra to identify the similarities and differences across the three platforms. In addition, PMF was applied to NEXAFS-STXM and FTIR spectra independently to identify the contributions of some general classes of sources to the organic particles. The emitted particles are defined as organic components formed directly from the emissions of one source type, and the processed particles are defined as organic components formed by multiple source or atmospheric components (Russell et al., 2009). This work illustrates important differences in the characteristics of the organic mixtures from biomass burning, fossil fuel combustion, and atmospherically-processed sources for SIMAT, Altzomoni, and C130 flight measurements, and the analysis quantifies the approximate contribution of each source type to OM in the MCMA and surrounding areas.

2 Methods

Submicron particles were collected on Teflon filters in March 2006, during the MIRAGE (Megacity Impacts on Regional and Global Environments)/MILAGRO field campaign. The SIMAT site is located at the Mexico City Atmospheric Monitoring System building (19°25′ N, 99°7′ W), and the Altzomoni site is located about 60 km southeast of Mexico City, in the Pass of Cortez between the volcanoes of Popocatépetl and Iztaccíhuatl (19°7′ N, 98°38′ W; Baumgardner et al., 2009). The sample collection, FTIR analysis of organic functional group concentrations, and XRF analysis for SIMAT, Altzomoni, and the NCAR C130 platforms are described in a companion paper by Gilardoni et

al. (2009). The FTIR spectra were quantified as mass concentrations of organic functional groups using an automated algorithm (Russell et al., 2009), including additional calibrations of primary amine functional groups (Appendix A) in addition to standard compound calibrations presented in previous work (Maria et al., 2002, 2003, 2004; Maria and Russel, 2005; Gilardoni et al., 2007).

Elements heavier than Na were analyzed by Chester Laboratories on the same filters used for the FTIR analysis (Maria et al., 2003). Elemental concentrations reported were above detection for more than 70% of the ambient samples collected. The elements Mg, P, Co, Ga, Ge, As, Rb, Sr, Y, Zr, Mo, Pd, Ag, Cd, In, Sb, La, and Hg were always below detection limits. A data matrix was constructed including organic functional group concentrations and elemental concentrations for each sample filter. Correlations of each pair of components were calculated to provide the covariance of these aerosol components and investigate possible sources.

Normalized FTIR spectra of three platforms were grouped into clusters using the Agglomerative Hierarchical Clustering technique with the Ward algorithm. In this algorithm, each spectrum is initially considered as a separate category, a dendrogram is built from the spectra by progressively merging them and minimizing the sum-of-square errors for the spectra being merged (ultimately resulting in all spectra collapsing into one single category). The dendrogram can be grouped into clusters by choosing a level of branching that results in a meaningful number of categories (Kaufman et al., 1990). In this work, seven clusters were selected.

Positive matrix factorization (PMF) was applied to the total 263 mass-weighted FTIR spectra of three platforms (Paatero et al., 1994; Russell et al., 2009). PMF can be used to infer unknown source profiles and source contributions from ambient data (Lee et al., 1999; Ramadan et al., 2000). The rotation parameters and the number of factors were explored. The rotation parameter FPEAK was set to −0.2, 0, 0.2, and 0.4 for 3, 4, 5, and 6 factors. The effects of rotation were small, and FPEAK=0 was used. Singular value decomposition was applied to the entire data set for the determination of the number of factors. Three to six factors were found to reproduce 95–99% of

the data set and to generate reasonable factors, with the largest difference in factor concentrations occurring between the 3-factor results and the 4, 5, and 6-factor results. The output sample contribution factor was normalized by volume and correlated to metal concentrations to identify sources most likely associated with each factor.

Potential Source Contribution Function (PSCF; Pekney et al., 2006) was used to determine the most probable potential source regions to each PMF factor. PSCF calculates the probability that a source is located at a particular geographical region. 8-h (hourly) backtrajectories originating from the SIMAT coordinates were computed for the entire campaign using the Hybrid Single-Particle Lagrangian Integrated Trajectory (HYSPLIT) model. These trajectories were grouped into periods in which PMF source contributions were either high or low. Periods in which the source contribution for each factor was higher than its 75th percentile value were classified as high periods, and the rest of the periods were classified as low. The trajectories were interpolated into 15-min intervals and superposed on a 4 (latitude)×4 (longitude) degree domain centered around the city and gridded into a total of 250 000 cells. Frequencies for high and low periods were normalized by total counts for each grid cell for the PSCF analysis (Pekney et al., 2006).

Particles were also collected on silicon nitride windows, and single particle K-edge X-ray absorption spectra were acquired using a combination of Scanning Transmission X-ray Microscopy (STXM) and Near-Edge X-ray Absorption Fine Structure (NEXAFS) spectroscopy at the Lawrence Berkeley National Laboratory Advanced Light Source on beam line 5.3.2 (Russell et al., 2002; Maria et al., 2004). PMF was applied to the total 270 NEXAFS-STXM spectra of SIMAT and C130 measurements. The rotation parameters and the number of factors were explored. The rotation parameter FPEAK was set to −0.2, 0, 0.2 and 0.4 for 2 to 8 factors. Two to eight factors were found to reproduce 85–99% of the data set. 4-factor solution with FPEAK set to 0 was found to produce the most representative results.

3 Results

The average OM concentrations at STP were 9.9 $\mu g\,m^{-3}$ at SIMAT, 6.6 $\mu g\,m^{-3}$ at Altzomoni, and 5.3 $\mu g\,m^{-3}$ on the C130 (Gilardoni et al., 2009). Alkane functional groups dominated the total OM, with the mass fractions 47%, 41%, and 73% for SIMAT, Altzomoni, and C130 measurements, respectively. Carboxylic acid functional groups contributed 30% and 28% to OM at SIMAT and Altzomoni, with a lower fraction of 5% on average for the C130 flights. Alcohol functional groups accounted for 14% of OM at SIMAT, with larger fractions of 19% both at Altzomoni and on the C130. The mass fractions of primary amine functional groups were 9% at SIMAT, 11% at Altzomoni, and 2% on the C130 (Table 1). Of the C130 samples, 87% of amine functional group masses and 73% of carboxylic acid functional group masses were below detection limit, and typically could have accounted for up to 1% and 15% of OM, respectively. FTIR spectra were analyzed for evidence consistent with organosulfate functional groups, but no samples had detectable absorbance at 876 cm^{-1}. Alkene and aromatic functional group masses were below detection limit in all samples of the three platforms, accounting for less than 1% of the average OM. All of the normalized and fractional quantities in the following discussion omit these two functional groups.

The Oxygen-to-Carbon ratio (O/C) can be estimated from FTIR measurements (Russell et al., 2009). The average FTIR O/C was 0.4 for SIMAT, and this value is comparable to the AMS O/C=0.41 at the nearby T0 sampling site (9 km northeast of SIMAT sampling site) from AMS-based estimates (Aiken et al., 2008). The FTIR O/C was compared with the O/C calculated from quadrupole AMS (Aerosol Mass Spectrometer) measurements using the reported ambient relationship for m/z 44 (Aiken et al., 2008; Shilling et al., 2008) for Altzomoni and C130 platforms. At Altzomoni, the FTIR O/C was consistently lower than the AMS O/C, but the differences were within the uncertainties of both FTIR and AMS. On the C130, the FTIR O/C and AMS O/C compared well for the samples with carboxylic acid functional groups above detection limit. These comparisons are consistent with the previous study (Russell et al., 2009), showing that

ACPD
9, 4567–4607, 2009

the O/C estimates from FTIR and AMS are within the uncertainties associated with inlet transmission. The standard deviations of FTIR O/C were 0.07, 0.12, and 0.18 for SIMAT, Altzomoni, and C130 measurements, respectively. The larger O/C variation during the NCAR C130 flights indicates that the larger altitude and geographic range of these measurements show greater variability in organic composition than either of the two ground sites.

3.1 Correlations in concentrations

The SIMAT measurements show correlations of elemental markers from four types of sources: dust elemental markers (Al, Si, Ca, Ti, Fe) correlated with each other, with correlation coefficients (r) ranging from 0.5 to 0.9; S and Se were correlated with r of 0.55, indicating coal combustion source types (Qureshi et al., 2006); V and Ni are indicators of oil combustion, they were correlated with r of 0.87 (Qureshi et al., 2006); K and Br were correlated with r of 0.71, probably associated with biomass burning sources (Turn et al., 1997). Concentrations of alcohol, alkane, amine, and carboxylic acid functional groups correlated with each other as well as K, suggesting their common biomass burning origins. Alkane and carboxylic acid group mass fractions correlated with each other, but they anti-correlated with alcohol group mass fraction (Fig. 1a).

At Altzomoni, the dust elemental markers Al, Si, Ca, Ti, Fe, and Mn were correlated with each other with r ranging from 0.6 to 1.0, and combustion elemental markers V, S, K, Br, Pb, Se were correlated with each other with r ranging from 0.5 to 0.7 (Fig. 1b). The high correlations of the dust elemental concentrations may be caused by the single-lane local road, which is located 5 km southeast from Altzomoni site (Baumgardner et al., 2009). Compared to SIMAT and other urban sites (Russell et al., 2009), the combustion-generated components do not fall into clear fuel-specific combustion categories, consistent with higher contributions of more processed or mixed-source organic mass at Altzomoni. This result is also consistent with a higher O/C and OM/OC at Altzomoni than at SIMAT. Concentrations of alkane, amine, and carboxylic acid functional groups correlated with each other as well as S and K, indicating that sulfur emissions

may also have been oxidized from SO_2 to form sulfate during atmospheric processing. Similar to SIMAT, alkane and carboxylic acid group mass fractions were correlated with each other but were anti-correlated with alcohol group mass fractions.

Dust elemental markers Si, Ca, and Fe were correlated with each other, with *r* ranging from 0.5 to 0.6 in the C130 data set; Ca also correlated with combustion type elements S, K, and V with *r* of 0.4, 0.5 and 0.6, respectively (Fig. 1c), indicating particles from mixed source types. The correlations between organic functional groups and elements were weak, indicating that the particles were mixed or processed during atmospheric transport, leaving no clear source signature. Concentrations of alcohol and alkane functional groups correlate with each other, but the mass fractions of alcohol and alkane functional groups were anti-correlated.

3.2 Cluster analysis of FTIR spectra

Cluster analysis was used to identify similarities among the measured normalized FTIR spectra. The Ward-type cluster analysis method was used and two to seven branches were tested. Spectra from the C130 measurements were separated from the Altzomoni and SIMAT spectra at the first branch; Altzomoni spectra started to be separated out when five or more branches were used. Seven clusters were used to represent the different types of the spectra (Fig. 2).

Clusters I, II, and III are the dominant clusters, as they contain 65% of the spectra. Seventy-percent of the spectra from clusters I and III are from SIMAT and the other 30% are from Altzomoni, with the difference between these two clusters being the presence of a sharper peak in the alkane functional group region of cluster III spectra. Samples from cluster III also have the lowest O/C among clusters I-IV. Forty-percent of the spectra in cluster II are from SIMAT and 45% from C130 measurements. The C130 samples in this cluster were collected at lower altitudes and closer to the Mexico City basin than the samples in the other clusters, indicating these samples were influenced by the city outflow. The similarities among spectra from different platforms suggest that many of the sources are associated with region-wide pollution that is transported in air masses

sampled by all three platforms, which is consistent with the findings of Baumgardner et al. (2009). 85% of the spectra in cluster IV are from Altzomoni and 15% from SIMAT. The average O/C of the samples in cluster IV is significantly higher (at a 95% confidence level) than O/C of the samples in the other clusters. Clusters V, VI, and VII consist almost exclusively of C130 spectra, with only 5% of the spectra from Altzomoni in cluster V. The three distinct branches of clusters of C130 measurements separated from the ground site measurements indicates the wide variety of different sources and air masses sampled by the C130.

3.3 Positive matrix factorization of FTIR spectra

PMF was used to divide organic functional group concentrations into three to six factors, with the time series of OM concentrations for PMF factors shown in Fig. 3. The apportionment of OM concentrations and OC-weighted O/C to the factors are shown in Fig. 4. The functional group concentrations of these factors are summarized in Table 2 for SIMAT, Altzmoni and C130 measurements. The OM concentration of each factor was correlated with the corresponding elemental concentrations to show the contributions of different source types to organic functional groups. For each factor, correlations to elements with $r>0.53$ and $0.4<r<0.53$ are listed in Table 2.

The correlations and PSCF results show that the same factors were consistently found in all PMF runs. Factors 1, 3, and 4 were identified as fossil fuel combustion type factors (which we will call combustion I, II, and III) because they were associated with more than one metal associated with fossil fuel combustion. Similar metal combustion tracers are associated with these factors. Factor 1 correlates with Fe, Br, and Mn with $0.4<r<0.53$. Factor 3 correlates with S ($r>0.53$), and Se, Zn, and Mn with $0.4<r<0.53$. Factor 4 correlates with Br ($r>0.53$) and S ($0.4<r<0.5$). These elements can be attributed to various combustion processes, such as oil burning, coal burning, solid waste incineration, and motor vehicle emissions (Sharma et al., 2005; Li et al., 2004; Balasubramanian et al., 2004; Finlayson-Pitts et al., 2000). The combustion sources around Mexico City include incineration (Moffet et al., 2008a), oil combustion

(Moffet et al., 2008b), motor vehicle emissions (Vega et al., 1997; Chow et al., 2002; Querol et al., 2008; Stone et al., 2008), and local charcoal burning (CICA, 1999), which can produce the elements associated with these three factors. Factor 3 (combustion factor II) in the 3-factor PMF run splits to factor 3 and factor 4 (combustion factor III) in the 4-factor PMF run (Fig. 4), since both the spectrum and the OM of factor 3 in the 3-factor PMF run are approximately the combinations of the spectra and OM of factor 3 and factor 4 in the 4-factor PMF run. Factors 3 and 4 are consistent through 4, 5, and 6-factor PMF runs. While some studies showed the diurnal trend and weekday or weekend variations of OC (Stone et al., 2008), none of these factors were found to have these patterns. The similarities of the trace metal signatures, the variety of fuels used in Mexico City, the splitting of factor 3 into two very similar factors result in no clear fuel type for these combustion sources. Although no specific sources are assigned to these factors, the air mass back trajectories and OM concentrations provide some information about the differences among the combustion type factors. Combustion factor I has no specific geographic regions associated with the back trajectories correlated to this factor, and the OM concentration associated with this factor is approximately ten times lower than the other two combustion type factors.

Alkane and carboxylic acid functional groups dominate combustion factor II, accounting for 54–65% and 19–29% of the total OM concentration, respectively. High OM concentrations of combustion factor II originate from northeast of the SIMAT sampling site, indicating the influence of the incineration process from the northeast (Moffet et al., 2008a). The OM contribution by combustion factor II at SIMAT is about 1.5 times larger than at the other two platforms. This factor has the lowest O/C ratio of all factors as a result of its large mass fraction of alkane functional groups and relatively small mass fraction of alcohol functional groups. High OM concentrations of combustion factor III originate from northwest of the SIMAT site. Compared to combustion factor II, the OM differences for combustion factor III among the three platforms are small. The alkane functional group dominates in this factor, accounting for 47–51% of the total OM.

The second factor has almost no correlation with any of the elements, and has the

ACPD
9, 4567–4607, 2009

highest O/C among all factors, with the average O/C ranging from 0.8–1.2. This second factor is identified as a mixed or processed emissions factor. The OM contribution of this factor is the largest at Altzomoni, showing more processed particulate masses at the high altitude rural site. The alcohol functional group dominates in this factor, accounting for 43–68% of the total OM, indicating that more oxygenated organic compounds are formed during atmospheric processing. The alkane group is the second largest group, and it accounts for 12–23% of the total OM.

The fifth factor correlates with K, Br, Mn, and Fe (r>0.53), and these elements can be from biomass burning (Turn et al., 1997; Gaudichet et al., 1995; Guieu et al., 2005; Luo et al., 2008; Reimann et al., 2008). This factor is identified as a biomass burning factor because K is an indicator of biomass burning (Johnson et al., 2006) and the OM of this factor is significantly higher at the 95% confidence level during the high fire periods than during the no fire periods described by Aiken et al. (2009). These results are consistent with the effects of biomass burning events on the organic mass concentrations of Mexico City described elsewhere (Moffet et al., 2008b; Gilardoni et al., 2009). Alkane and non-carboxylic acid carbonyl functional groups dominate the OM, as they account for 32–33% and 34–36%, respectively. The OM contribution of this factor at SIMAT is twice as large as the OM contribution of this factor at Altzomoni, indicating that biomass burning has a larger influence on the urban area than on the southern Altzomoni site during the MILAGRO campaign.

The sixth factor is identified as a C130 factor since the OM associated with this factor is a large fraction of the C130 measurements and is negligible for the other two platforms. This factor may be representative of low-particle-loading sample spectra. The alkane group dominates in this factor and accounts for 61% of the total OM measured on the C130.

3.4 PMF and clusters of NEXAFS-STXM spectra

Three factors were consistently observed in 80% of all PMF runs. These factors were interpreted by comparing them with reference NEXAFS-STXM spectra of pure com-

pounds and typical types of NEXAFS-STXM spectra identified in atmospheric particle measurements described by Takahama et al. (2007).

The first factor spectrum shows ketone and alkene group absorption peaks at 285 eV and 287.7 eV. This factor is identified as a soot factor, as the shape of this factor spectrum is comparable with the soot type spectra described by Braun et al. (2005) and Hopkins et al. (2007). The second factor spectrum is dominated by a strong carboxylic acid absorption peak at 288.7 eV and shares similarities with the spectra of category (a) described by Takahama et al. (2007). Particles in category (a) are likely from secondary organic aerosol formation, so this factor is identified as an atmospherically-processed factor. Factor 3 compares well with fulvic acid spectrum (Ade et al., 2002). Fulvic acid in atmospheric particles are likely to originate from biomass burning events (Tivanski et al., 2007), thus this factor is identified as a biomass burning factor (Fig. 5). The 4-factor solution with a rotation of 0 resulted in the most representative results. This solution contains the three main factors identified above and an additional factor, which was present in only a few particles. The three main factors account for 80% of the particles analyzed by NEXAFS-STXM for the SIMAT and C130 during MILAGRO.

NEXAFS-STXM spectra were grouped into "secondary" type, "biomass burning" type, and "soot" type spectra described by Takahama et al. (2007). Figure 6 summarizes the size distributions of analyzed particles and the average fractions of the three major factors within each size range. The "secondary" type particles are in the size range of 0.2–5 μm, while the "biomass burning" and "soot" type particles are in the size range of 0.1–10 μm. The "soot" type particles are the most abundant, and 70% of these particles have diameters falling between 0.2 and 1 μm. The soot factor is the largest factor for particles smaller than 1 μm, and its fractions are lower in large size ranges. The "processed" factor shows an increased fraction from 0.1–0.2 μm to 0.2–0.5 μm size ranges, and the fractions are nearly constant for particles larger than 0.2 μm. Figure 7a shows that the contributions of soot and biomass burning factors to each ambient particle spectrum vary, but most particles show consistent contributions from processing. The processed factor accounts for 10%–60% of the carbon

absorbance, while the fractions of the other two factors show a larger variation ranging from about 0%–60% and 0%–80%, suggesting the biomass burning and black carbon factors are more source-related, while the processed factor has a consistent contribution to most particles.

4 Discussion

In this section, we consider how the organic mass and oxygenated fraction of organic mass are affected by diurnal trends at three platforms. We also use the FTIR spectral clusters to highlight the differences observed among the three platforms. Our PMF analysis provides a way to link some of these differences in measurements from the three platforms to the types of sources that affect each. In addition, we compare and contrast our results from NEXAFS-STXM spectra from single particle measurements and FTIR spectra from submicron bulk particle samples.

4.1 Diurnal trend of functional groups and elements

Samples were divided into "morning", "afternoon", and "night" categories according to the sampling time to investigate the differences of organic functional groups and elements as a function of time of day. Tukey's Honest Significant Difference method was applied to calculate the differences of the mean concentrations among the categories at a 90% confidence level.

At SIMAT, concentrations of OM, alkane and carboxylic acid functional groups, and As were found to be significantly higher in the morning than in the afternoon or at night. As may be from charcoal burning by street vendors and others in Mexico City (Kitamura et al., 2000; CICA, 1999). The high OM and organic functional group concentrations could be explained by either the emission of compounds containing alkane and carboxylic acid functional groups by traffic in the morning or by the low boundary layer in the early morning (Shaw et al., 2007). OM/OC and O/C is significantly higher

in the afternoon, indicating that photochemical processes may contribute to the oxidation of organic compounds in the afternoon. Fractions of alcohol and carboxylic acid functional groups have higher values at night than in the afternoon, possibly indicating the relative reduction of alkane functional groups and the concomitant accumulation of oxygenated compounds emitted and produced during the day.

At Altzomoni, concentrations of alkane groups, carboxylic acid groups, amine groups, Se, V, K, and S were found to be higher during the day than at night. Back trajectories at Altzomoni show that the air masses mainly came from east and southeast during daytime. The city of Puebla, which is located approximately 50 km east of Altzomoni, is the fourth most populous city in the country, and it has intense vehicular traffic as well as an important industrial zone in its metropolitan area (Juarez et al., 2005). The boundary layer can reach as high as 6 km during the day (Shaw et al., 2007), which is higher than the 4010 m location of the Altzomoni site. The elevated concentrations of those species during the day may be caused by the transport of pollutants from Puebla. During the night, the boundary layer decreased, and the site was influenced by air masses in the free troposphere, resulting in low concentrations at night.

No significant differences were found between the morning and afternoon for the C130 measurements, which is not surprising as the measurements are sparse and the sampling location for each observation varied on this mobile platform. While other studies have found that there are coarse particle concentration differences between weekdays and weekends (Stephens et al., 2008), differences in submicron organic functional group and elemental concentrations between days of the week were not found in this study for any platform.

4.2 FTIR spectral clusters and O/C

The shapes of spectra in cluster II are comparable to the spectral shapes in cluster S1 identified in shipboard measurements during TexAQS/GoMACCS 2006 near Houston (Russell et al., 2009). Sample spectra in cluster S1 were mainly from the relatively clean southerly flow from the Gulf or polluted by some nearby land-based sources.

The similarities of the spectra from different geographical locations indicate that there are some common sources or processes occurring in the atmosphere.

Cluster I and cluster III mainly consist of spectra from SIMAT and Altzomoni, reflecting the similarities of submicron organic composition at these two platforms during certain time periods. Back trajectories at Altzomoni show that the air masses mainly came from northeast, east, and southeast of the site for samples in cluster I and cluster III, indicating the influence of urban pollution from Puebla and biomass burning episodes (Baumgardner et al., 2009). Puebla and Mexico City may have similar pollution sources, such as vehicular traffic and industrial zones (Juarez et al., 2005), and biomass burning is a large contributor of OM in Mexico City. It is possible that the transport of Puebla plumes and biomass burning particles to Altzomoni results in organic particles with similar composition at Altzomoni and SIMAT.

Alkane, carboxylic acid, and alcohol groups are the main functional groups in particles and they account for more than 80% of OM for three platforms. Figure 8 shows the distributions of clustered spectra as a function of alkane, carboxylic acid, and alcohol group mass fractions. At SIMAT, the clustered spectra are relatively centered on the triangle plot, showing comparable mass fractions of the three main functional groups. At Altzomoni, cluster IV is separated from other clusters. Samples from cluster IV show high alcohol group concentrations, and the highest O/C. Spectra from this cluster are mainly from Altzomoni (Fig. 2) during times when the wind direction was from the north or northwest bringing air from Mexico City (Gilardoni et al., 2009), suggesting that cluster IV spectra may be associated with processed particles that originated in Mexico City.

4.3 PMF factors and associated sources

PMF factors attribute alkane and carboxylic acid groups largely to combustion type sources. This supports the findings that fossil fuel combustion processes, such as gasoline combustion, oil burning, and coal burning are sources of alkane and carboxylic acid groups in atmospheric particles (Rogge et al., 1993; Oros et al., 2000).

Amines have been suggested to originate from motor vehicle exhaust, biomass burning, industrial processes, and marine organisms (Murphy et al., 2007). PMF attributes the main source of amine to combustion type sources, which is consistent with the possible motor vehicle source discussed by Moffet et al. (2008b).

The processed factor is associated with the highest fraction of alcohol functional group among all factors. The OM contribution of this factor is two to three times larger at Altzomoni than at SIMAT or C130. Alcohol functional groups in atmospheric particles may come from gas-to-particle conversion during particle processing, so they are likely to be associated with a mixture of sources that have been processed in the atmosphere, resulting in only weak correlations to trace metals. Photochemical aging of OM have been observed in Mexico City in other studies (Moffet et al., 2008b), including evidence that secondary particles accounted for a large fraction of OC (Stone et al., 2008). This factor is likely to be dominated by atmospheric processing.

Half of the O/C in the measured ambient aerosol is attributed by the PMF results to the fossil fuel combustion emissions, and one-third of the O/C is attributed to atmospheric processing. For example, the 4-factor PMF run of Altzomoni measurements attributes 2.9 $\mu g\,m^{-3}$ to combustion III type emissions with O/C of 0.4 and 2.3 $\mu g\,m^{-3}$ to combustion II type emissions with O/C of 0.30, which together account for half of the total 8.0 $\mu g\,m^{-3}$ average concentration and O/C of 0.47 (Fig. 4). The processed factor has the O/C of 0.8 and OM of 2.3 $\mu g\,m^{-3}$, and it accounts for about one-third of the average O/C. This result indicates that the O/C at Altzomoni is largely the result of emissions rather than processing. Similar relationships hold for SIMAT and C130 measurements. This attribution of a majority of the oxygenated organic components to direct emission sources rather than processing is consistent with the findings of Tex-AQS/GoMACCS (Russell et al., 2009). The high O/C of cluster IV of FTIR spectra suggests that particles associated with cluster IV are likely rapidly oxidized after being emitted.

ACPD
9, 4567–4607, 2009

4.4 Comparison of NEXAFS-STXM and FTIR factors from PMF

While the single-particle NEXAFS-STXM spectra are sparse in terms of particle number and sampling times, the submicron particle types that are frequently identified are expected to have some organic components that are similar to the composition of submicron particle mass collected on bulk filters. Figure 7b shows the fractions of combined fossil fuel combustion factors, the processed factor, and the biomass burning factor of FTIR samples from SIMAT and C130 platforms. Clusters V and VII are associated with highly processed factor fractions, and they are separated from the other clusters. Clusters II and III are separated: cluster II is associated with larger fossil fuel combustion factor fractions, while cluster III is associated with larger biomass burning factor fractions. Results from single particle spectra show that the soot type particles are separated from biomass burning type particles (Fig. 7a). This indicates some clusters of both single particle spectra and bulk particle spectra are source-related. Figure 7b also shows that 95% of the fractions of the processed factor vary from 0–40%, while the fractions of the fossil fuel combustion factors and the biomass burning factor are in the range of 30–100% and 0–50%, respectively. Both results show that the processed factor is more consistent during the sampling period than the combustion factors, since it has a smaller range of contribution for most particles.

5 Conclusions

Organic mass concentrations were 9.9 $\mu g\,m^{-3}$, 6.6 $\mu g\,m^{-3}$, and 5.3 $\mu g\,m^{-3}$ for SIMAT, Altzomoni, and C130 flight measurements. Alkane functional group concentrations dominated the mass, with the fractions ranging from 41% to 73%. Dust markers Ca, Fe, and Si correlated with each other for all three platforms, while combustion type elements showed different correlations among the three platforms. At SIMAT, three source-related groups of elements were identified: coal combustion type elements (S and Se), oil combustion type elements (V and Ni), and biomass burning type elements

ACPD
9, 4567–4607, 2009

(K and Br); while at Altzomoni, elements from several types of fossil fuel combustion (V, S, K, Br, Pb, Se) correlated with each other. For the C130 measurements, Ca was found to correlate with S, K, and V. The differences in correlations of elements among the three platforms suggest that the urban area was more influenced by fresh emissions, while the high altitude site was more influenced by mixed sources or atmospheric (photochemical) processing. However, even at Altzomoni, processing accounted for only a third of O/C.

The cluster analysis of FTIR spectra shows both similarities and differences among the three platforms. Seven distinct clusters of FTIR spectra were identified, from which the last three clusters consist almost exclusively of samples collected aboard the C130 research flights based in Veracruz, indicating the wide variety of different sources and air masses sampled by the C130. More than 80% of SIMAT spectra and more than 70% of Altzomoni spectra are identified as clusters I and III, while cluster IV consists almost exclusively of Altzomoni spectra with high alcohol group fractions. The easterly and southeasterly transport of Puebla pollutants and biomass burning particles to Altzomoni may result in the similarities of organic particles from Altzomoni and SIMAT, while the distinct cluster IV of Altzomoni samples with high O/C suggests more processed particles at Altzomoni site than at the SIMAT site.

PMF analysis was applied to NEXAFS-STXM spectra and FTIR spectra. PMF of NEXAFS-STXM spectra resulted in three main factors, which represent biomass burning, processed, and fossil fuel combustion type spectra. PMF of FTIR spectra resulted in three fossil fuel combustion type factors, one biomass burning factor, and one processed factor. Several trends in composition were consistent for the factors and rotations selected. Alkane groups have the largest fractions in the two major combustion type factors and the biomass burning factor, suggesting the alkane groups mostly originate from primary sources. Carboxylic acid and amine groups were also associated with combustion emissions. Alcohol group mass fractions of 43–68% were associated with the "processed" factor, which has high O/C and is the largest contributor to alcohol group concentration. In addition, the "processed" factor has a higher contribution for

ACPD
9, 4567–4607, 2009

Altzomoni than for SIMAT and C130 measurements, indicating alcohol groups were associated with atmospheric oxidation processes that occurred downwind over longer time scales. All of the PMF results suggest that while the processed aerosol has the highest O/C, half of the O/C is associated with the fossil fuel combustion type emissions. This result indicates that the high O/C from Altzomoni is largely the result of direct emissions rather than processing. This finding also holds for the SIMAT and C130 measurements. Both PMF of single particle spectra and PMF of bulk sample spectra show that the clusters are associated with different fractions of the factor contributions. A narrower range of 0 to 60% of processed factor fractions than combustion type factors suggests that the combustion type factors (0–100%) vary more with local source contributions, while the processed factor is more consistent during the sampling period on all three platforms.

Appendix A

FTIR calibrations of amine functional groups

Calibrations of organic functional groups of FTIR spectra were conducted using the measured absorption per mole of each component from laboratory-generated standards (Maria et al., 2002). Three primary amine standards (n-Tridecylamine, n-Tetradecylamine, alanine) and three secondary amine standards (N-Methyl-n-octadecylamine, Di-n-decylamine, Di-n-dodecylamine) were used to quantify amine functional group absorption at 1625 cm^{-1} observed in our ambient particle spectra. Results showed that secondary amines do not have detectable absorption peaks at 1625 cm^{-1}. Alanine was used as the standard for quantification of primary amine groups as it best represents the absorption peak at 1625 cm^{-1}. The revised guided algorithm (Russell et al., 2009) was applied to do peak fitting and integration of alanine standard spectra. The absorptivity of amine functional group is 0.12 μmol/unit of peak area, with a linear fit (R^2=0.97) of absorption and moles per functional group.

ACPD
9, 4567–4607, 2009

Deviations from this absorptivity were not observed for mixtures of alanine and ammonium sulfate. Possibilities of absorption at 1625 cm^{-1} by organonitrate compounds were ruled out by the absence of absorption at 1280 cm^{-1} in the ambient FTIR spectra (Mylonas et al., 1991; Allen et al., 1994; Garnes et al., 2002; Laurent et al., 2004). Water absorption at 1625 cm^{-1} is removed by purging the sample chamber of FTIR instrument for 3 min before scanning each sample.

Acknowledgements. The authors appreciate the funding from DOE (Department Of Energy W/GEC05-010 and MPC35TA-A5) and NSF (National Science Foundation ATM-0511772).

References

Ade, H. and Urquhart, S. G.: NEXAFS spectroscopy and microscopy of natural and synthetic polymers, in: Chemical Applications of Synchrotron Radiation, World Scientific Publishing, Singapore, 285–355, 2002.

Aiken, A. C., Decarlo, P. F., Kroll, J. H., Worsnop, D. R., Huffman, J. A., Docherty, K. S., Ulbrich, I. M., Mohr, C., Kimmel, J. R., Sueper, D., Sun, Y., Zhang, Q., Trimborn, A., Northway, M., Ziemann, P. J., Canagaratna, M. R., Onasch, T. B., Alfarra, M. R., Prevot, A. S. H., Dommen, J., Duplissy, J., Metzger, A., Baltensperger, U., and Jimenez, J. L.: O/C and OM/OC ratios of primary, secondary, and ambient organic aerosols with high-resolution time-of-flight aerosol mass spectrometry, Environ. Sci. Technol., 42(12), 4478–4485, 2008.

Aiken, A. C. and Jimenez, J. L.: Mexico City Aerosol Analysis during MILAGRO using High Resolution Aerosol Mass Spectrometry at the Urban Supersite (T0), Part 2: Intercomparison of Source Apportionment Methods, Atmos. Chem. Phys. Discuss., in preparation, 2009.

Allen, D. T., Palen, E. J., Haimov, M. I., Hering, S. V., and Young, J. R.: Fourier-Transform Infrared-Spectroscopy Of Aerosol Collected In A Low-Pressure Impactor (Lpi/Ftir) – Method Development And Field Calibration, Aerosol Sci. Tech., 21(4), 325–342, 1994.

Balasubramanian, R. and Qian, W. B.: Characterization and source identification of airborne trace metals in Singapore, J. Environ. Monitor., 6(10), 813–818, 2004.

Baumgardner, D., Grutter, M., Allan, J., Ochoa, C., Rappenglueck, B., Russell, L. M., and Arnott, P.: Evolution of anthropogenic pollution at the top of the regional mixed layer in the central Mexico plateau, Atmos. Chem. Phys. Discuss., in press, 2009.

Braun, A., Shah, N., Huggins, F. E., Kelly, K. E., Sarofim, A., Jacobsen, C., Wirick, S., Francis, H., Ilavsky, J., Thomas, G. E., and Huffman, G. P.: X-ray scattering and spectroscopy studies on diesel soot from oxygenated fuel under various engine load conditions, Carbon, 43(12), 2588–2599, 2005.

Chow, J. C., Watson, J. G., Edgerton, S. A., and Vega, E.: Chemical composition of $PM_{2.5}$ and PM_{10} in Mexico City during winter 1997, Sci. Total Environ., 287(3), 177–201, 2002.

CICA: Emissions from Street Vendor Cooking Devices (Charcoal Grilling), EPA-600/R- 99-048, available at: http://www.epa.gov/ttn/catc/dir1/mexfr.pdf(last access: 29 January 2009), 1999.

DeCarlo, P. F., Dunlea, E. J., Kimmel, J. R., Aiken, A. C., Sueper, D., Crounse, J., Wennberg, P. O., Emmons, L., Shinozuka, Y., Clarke, A., Zhou, J., Tomlinson, J., Collins, D. R., Knapp, D., Weinheimer, A. J., Montzka, D. D., Campos, T., and Jimenez, J. L.: Fast airborne aerosol size and chemistry measurements above Mexico City and Central Mexico during the MILAGRO campaign, Atmos. Chem. Phys., 8, 4027–4048, 2008, http://www.atmos-chem-phys.net/8/4027/2008/.

Dockery, D. W., Pope, C. A., Xu, X. P., Spengler, J. D., Ware, J. H., Fay, M. E., Ferris, B. G., and Speizer, F. E.: An Association Between Air-Pollution And Mortality In 6 United-States Cities, New Engl. J. Med., 329(24), 1753–1759, 1993.

Eidels-Dubovoi, S.: Aerosol impacts on visible light extinction in the atmosphere of Mexico City, Sci. Total Environ., 287(3), 213–220, 2002.

Finlayson-Pitts, B. J. and Pitts, J. N.: Chemistry of the Upper and Lower Atmosphere, Academic Press, San Diego, USA, 386–388, 2000.

Garnes, L. A. and Allen, D. T.: Size distributions of organonitrates in ambient aerosol collected in Houston, Texas, Aerosol Sci. Technol., 36(10), 983–992, 2002.

Gaudichet, A., Echalar, F., Chatenet, B., Quisefit, J. P., Malingre, G., Cachier, H., Buatmenard, P., Artaxo, P. and Maenhaut, W.: Trace-Elements In Tropical African Savanna Biomass Burning Aerosols, J. Atmos. Chem., 22(1–2), 19–39, 1995.

Gilardoni, S., Russell, L. M., Sorooshian, A., Flagan, R. C., Seinfeld, J. H., Bates, T. S., Quinn, P. K., Allan, J. D., Williams, B., Goldstein, A. H., Onasch, T. B., and Worsnop, D. R.: Regional variation of organic functional groups in aerosol particles on four US east coast platforms

during the International Consortium for Atmospheric Research on Transport and Transformation 2004 campaign, J. Geophys. Res.-Atmos., 112, D10S27, doi:10.1029/2006JD007737, 2007.
Gilardoni, S., Takahama, S., Liu, S., Russell, L. M., Allan, J. D., Baumgardner, D., Jimenez, J. L., Decarlo, P. F., and Dunlea, E.: Characterization of organic ambient aerosol during MIRAGE 2006 on three platforms, Atmos. Chem. Phys., in preparation, 2009.
Guieu, C., Bonnet, S., Wagener, T., and Loye-Pilot, M. D.: Biomass burning as a source of dissolved iron to the open ocean?, Geophys. Res. Lett., 32, L19608, doi:10.1029/2005GL022962, 2005.
Hopkins, R. J., Tivanski, A. V., Marten, B. D., and Gilles, M. K.: Chemical bonding and structure of black carbon reference materials and individual carbonaceous atmospheric aerosols, J, Aerosol Sci,, 38(6), 573–591, 2007.
Johnson, K. S., de Foy, B., Zuberi, B., Molina, L. T., Molina, M. J., Xie, Y., Laskin, A., and Shuthanandan, V.: Aerosol composition and source apportionment in the Mexico City Metropolitan Area with PIXE/PESA/STIM and multivariate analysis, Atmos. Chem. Phys., 6, 4591–4600, 2006, http://www.atmos-chem-phys.net/6/4591/2006/.
Juarez, A., Gay, C., and Flores, Y.: Impact of the Popocatepetl's volcanic activity on the air quality of Puebla City, Mexico, Atmosfera, 18(1), 57–69, 2005.
Kaufman, L. and Rousseeuw, P. J.: Finding Groups in Data: An Introduction to cluster Analysis, Wiley, New York, 45–48, 1990.
Kitamura, T. and Katayama, H.: Behavior of copper, chromium and arsenic during carbonization of CCA treated wood, Mokuzai Gakkaishi, 46(6), 587–595, 2000.
Laurent, J. P. and Allen, D. T.: Size distributions of organic functional groups in ambient aerosol collected in Houston, Texas, Aerosol Sci. Technol., 38, 82–91, 2004.
Lee, E., Chan, C. K., and Paatero, P.: Application of positive matrix factorization in source apportionment of particulate pollutants in Hong Kong, Atmos. Environ., 33(19), 3201–3212, 1999.
Li, Z., Hopke, P. K., Husain, L., Qureshi, S., Dutkiewicz, V. A., Schwab, J. J., Drewnick, F., and Demerjian, K. L.: Sources of fine particle composition in New York city, Atmos. Environ., 38(38), 6521–6529, 2004.
Liepert, B. G., Feichter, J., Lohmann, U., and Roeckner, E.: Can aerosols spin down the water cycle in a warmer and moister world?, Geophys. Res. Lett., 31, L06207, doi:10.1029/2003GL019060, 2004.

Luo, C., Mahowald, N., Bond, T., Chuang, P. Y., Artaxo, P., Siefert, R., Chen, Y., and Schauer, J.: Combustion iron distribution and deposition, Global Biogeochem. Cy., 22, GB1012, doi:10.1029/2007GB002964, 2008.

Maria, S. F., Russell, L. M., Turpin, B. J., and Porcja, R. J.: FTIR measurements of functional groups and organic mass in aerosol samples over the Caribbean, Atmos. Environ., 36(33), 5185–5196, 2002.

Maria, S. F., Russell, L. M., Turpin, B. J., Porcja, R. J., Campos, T. L., Weber, R. J., and Huebert, B. J.: Source signatures of carbon monoxide and organic functional groups in Asian Pacific Regional Aerosol Characterization Experiment (ACE-Asia) submicron aerosol types, J. Geophys. Res.-Atmos., 108(D23), 8637, doi:10.1029/2003JD003703, 2003.

Maria, S. F., Russell, L. M., Gilles, M. K., and Myneni, S. C. B.: Organic aerosol growth mechanisms and their climate-forcing implications, Science, 306(5703), 1921–1924, 2004.

Maria, S. F. and Russell, L. M.: Organic and inorganic aerosol below-cloud scavenging by suburban New Jersey precipitation, Environ. Sci. Technol., 39, 13, 4793–4800, 2005.

Moffet, R. C., Desyaterik, Y., Hopkins, R. J., Tivanski, A. V., Gilles, M. K., Wang, Y., Shutthanandan, V., Molina, L. T., Abraham, R. G., Johnson, K. S., Mugica, V., Molina, M. J., Laskin, A., and Prather, K. A.: Characterization of aerosols containing Zn, Pb, and Cl from an industrial region of Mexico City, Environ. Sci. Technol., 42(19), 7091–7097, 2008a.

Moffet, R. C., de Foy, B., Molina, L. T., Molina, M. J., and Prather, K. A.: Measurement of ambient aerosols in northern Mexico City by single particle mass spectrometry, Atmos. Chem. Phys., 8, 4499–4516, 2008b, http://www.atmos-chem-phys.net/8/4499/2008/.

Molina, L. T., Kolb, C. E., de Foy, B., Lamb, B. K., Brune, W. H., Jimenez, J. L., Ramos-Villegas, R., Sarmiento, J., Paramo-Figueroa, V. H., Cardenas, B., Gutierrez-Avedoy, V., and Molina, M. J.: Air quality in North America's most populous city - overview of the MCMA-2003 campaign, Atmos. Chem. Phys., 7, 2447–2473, 2007, http://www.atmos-chem-phys.net/7/2447/2007/.

Murphy, S. M., Sorooshian, A., Kroll, J. H., Ng, N. L., Chhabra, P., Tong, C., Surratt, J. D., Knipping, E., Flagan, R. C., and Seinfeld, J. H.: Secondary aerosol formation from atmospheric reactions of aliphatic amines, Atmos. Chem. Phys., 7, 2313–2337, 2007, http://www.atmos-chem-phys.net/7/2313/2007/.

Mylonas, D. T., Allen, D. T., Ehrman, S. H., and Pratsinis, S. E.: The Sources And Size Distributions Of Organonitrates In Los-Angeles Aerosol, Atmos. Environ. A-Gen., 25, 12, 2855–2861, 1991.

Oros, D. R. and Simoneit, B. R. T.: Identification and emission rates of molecular tracers in coal smoke particulate matter, Fuel, 79(5), 515–536, 2000.
Paatero, P. and Tapper, U.: Positive Matrix Factorization – A Nonnegative Factor Model With Optimal Utilization Of Error-Estimates Of Data Values, Environmetrics, 5(2), 111–126, 1994.
Pekney, N. J., Davidson, C. I., Zhou, L. M., and Hopke, P. K.: Application of PSCF and CPF to PMF-modeled sources of $PM_{2.5}$ in Pittsburgh, Aerosol Sci. Technol., 40(10), 952–961, 2006.
Querol, X., Pey, J., Minguillón, M. C., Pérez, N., Alastuey, A., Viana, M., Moreno, T., Bernabé, R. M., Blanco, S., Cárdenas, B., Vega, E., Sosa, G., Escalona, S., Ruiz, H., and Artíñano, B.: PM speciation and sources in Mexico during the MILAGRO-2006 Campaign, Atmos. Chem. Phys., 8, 111–128, 2008, http://www.atmos-chem-phys.net/8/111/2008/.
Qureshi, S., Dutkiewicz, V. A., Khan, A. R., Swami, K., Yang, K. X., Husain, L., Schwab, J. J., and Demerjian, K. L.: Elemental composition of $PM_{2.5}$ aerosols in Queens, New York: Solubility and temporal trends, Atmos. Environ., 40, S238–S251, 2006.
Raga, G. B., Baumgardner, D., Castro, T., Martinez-Arroyo, A., and Navarro-Gonzalez, R.: Mexico City air quality: a qualitative review of gas and aerosol measurements (1960–2000), Atmos. Environ., 35(23), 4041–4058, 2001.
Ramadan, Z., Song, X. H., and Hopke, P. K.: Identification of sources of Phoenix aerosol by positive matrix factorization, J. Air Waste Manage., 50(8), 1308-1320, 2000.
Reimann, C., Ottesen, R. T., Andersson, M., Arnoldusser, A., Koller, F., and Enqlmaier, P.: Element levels in birch and spruce wood ashes – green energy?, Sci. Total Environ., 393(2–3), 191–197, 2008.
Rogge, W. F., Hildemann, L. M., Mazurek, M. A., Cass, G. R., and Simoneit, B. R. T.: Sources Of Fine Organic Aerosol. 2. Noncatalyst And Catalyst-Equipped Automobiles And Heavy-Duty Diesel Trucks, Environ. Sci. Technol., 27(4), 636–651, 1993.
Russell, L. M., Maria, S. F., and Myneni, S. C. B.: Mapping organic coatings on atmospheric particles, Geophys. Res. Lett., 29(16), 2002.
Russell, L. M., Takahama, S., Liu, S., Hawkins, L. N., Covert, D. S., Quinn, P. K., and Bates, T. S.: Oxygenated fraction and mass of organic aerosol from direct emission and atmospheric processing collected on the R/V Ronald Brown during TEXAQS/GoMACCS 2006, J. Geophys. Res., in press, available at: http://aerosol.ucsd.edu/publications.html, 2009.

Salcedo, D., Onasch, T. B., Dzepina, K., Canagaratna, M. R., Zhang, Q., Huffman, J. A., DeCarlo, P. F., Jayne, J. T., Mortimer, P., Worsnop, D. R., Kolb, C. E., Johnson, K. S., Zuberi, B., Marr, L. C., Volkamer, R., Molina, L. T., Molina, M. J., Cardenas, B., Bernabé, R. M., Márquez, C., Gaffney, J. S., Marley, N. A., Laskin, A., Shutthanandan, V., Xie, Y., Brune, W., Lesher, R., Shirley, T., and Jimenez, J. L.: Characterization of ambient aerosols in Mexico City during the MCMA-2003 campaign with Aerosol Mass Spectrometry: results from the CENICA Supersite, Atmos. Chem. Phys., 6, 925–946, 2006, http://www.atmos-chem-phys.net/6/925/2006/.

Shilling, J. E., Chen, Q., King, S. M., Rosenoern, T., Kroll, J. H., Worsnop, D. R., DeCarlo, P. F., Aiken, A. C., Sueper, D., Jimenez, J. L., and Martin, S. T.: Loading-dependent elemental composition of α-pinene SOA particles, Atmos. Chem. Phys. Discuss., 8, 15343–15373, 2008, http://www.atmos-chem-phys-discuss.net/8/15343/2008/.

Sharma, M. and Maloo, S.: Assessment of ambient air PM_{10} and $PM_{2.5}$ and characterization of PM_{10} in the city of Kanpur, India, Atmos. Environ., 39(33), 6015–6026, 2005.

Shaw, W. J., Pekour, M. S., Coulter, R. L., Martin, T. J., and Walters, J. T.: The daytime mixing layer observed by radiosonde, profiler, and lidar during MILAGRO, Atmos. Chem. Phys. Discuss., 7, 15025–15065, 2007, http://www.atmos-chem-phys-discuss.net/7/15025/2007/.

Stephens, S., Madronich, S., Wu, F., Olson, J. B., Ramos, R., Retama, A., and Muñoz, R.: Weekly patterns of México City's surface concentrations of CO, NO_x, PM_10 and O_3 during 1986-2007, Atmos. Chem. Phys., 8, 5313–5325, 2008, http://www.atmos-chem-phys.net/8/5313/2008/.

Stone, E. A., Snyder, D. C., Sheesley, R. J., Sullivan, A. P., Weber, R. J., and Schauer, J. J.: Source apportionment of fine organic aerosol in Mexico City during the MILAGRO experiment 2006, Atmos. Chem. Phys., 8, 1249–1259, 2008, http://www.atmos-chem-phys.net/8/1249/2008/.

Takahama, S., Gilardoni, S., Russell, L. M., and Kilcoyne, A. L. D.: Classification of multiple types of organic carbon composition in atmospheric particles by scanning transmission X-ray microscopy analysis, Atmos. Environ., 41(40), 9435–9451, 2007.

Tivanski, A. V., Hopkins, R. J., Tyliszczak, T., and Gilles, M. K.: Oxygenated interface on biomass burn tar balls determined by single particle scanning transmission X-ray microscopy, J. Phys. Chem. A, 111(25), 5448–5458, 2007.

Turn, S. Q., Jenkins, B. M., Chow, J. C., Pritchett, L. C., Campbell, D., Cahill, T., and Whalen, S. A.: Elemental characterization of particulate matter emitted from biomass burning: Wind tunnel derived source profiles for herbaceous and wood fuels, J. Geophys. Res.-Atmos., 102(D3), 3683–3699, 1997.

Vega, E., Garcia, I., Apam, D., Ruiz, M. E., and Barbiaux, M.: Application of a chemical mass balance receptor model to respirable particulate matter in Mexico city, J. Air Waste Manage., 47(4), 524–529, 1997.

Table 1. Mean and standard deviation of OM, organic functional group concentrations, O/C and OM/OC ratios, and elemental concentrations for SIMAT, Altzomoni and C130 platforms measured by FTIR and XRF.

		SIMAT	Altzomoni	C130
	FTIR OM $\mu g\,m^{-3}$	9.9±4.4	6.6±3.9	5.3±4.2
	FTIR OM/OC	1.8±0.1	2.0±0.3	1.5±0.2
	FTIR O/C	0.4±0.1	0.5±0.1	0.2±0.2
FTIR Organic Functional Groups	Alcohol	1.5±1.0 (14%)	1.1±1.2 (19%)	1.1±1.3 (19%)
($\mu g\,m^{-3}$)	Alkane	4.6±2.0 (47%)	2.7±1.5 (41%)	3.4±2.0 (73%)
	Non-Acid Carbonyl	0.0±0.3 (0%)	0.1±0.3 (1%)	0.1±0.6 (0%)
	Amine	0.8±0.3 (9%)	0.7±0.5 (11%)	0.1±0.3 (2%)
	Carboxylic Acid	3.0±1.4 (30%)	2.0±1.1 (28%)	0.5±1.4 (5%)
XRF Elements	Na	91.3±93.2		
($ng\,m^{-3}$)	Al	51.2±63.5	50.8±86.3	124.5±111.9
	Si	132.6±125.5	133.8±248.8	134.9±108.1
	S	954.6±516.5	706.3±462.1	476.3±476.0
	Cl	40.9±40.1		
	K	167.5±86.5	160.2±105.3	96.7±60.3
	Ca	106.9±115.1	83.6±211.7	25.4±18.5
	Ti	4.5±4.3	3.2±4.6	
	V	7.8±14.0	2.3±2.6	9.5±9.8
	Cr	0.9±1.2		
	Mn	4.3±4.4	0.9±1.7	
	Fe	92.9±73.4		25.9±23.4
	Ni	1.6±2.7		
	C	9.6±10.9		
	Zn	36.4±29.3		15.1±11.6
	Se	3.3±4.6		
	Br	6.3±7.6	2.9±1.6	
	Sn	6.6±7.3		68.5±69.4

ACPD
9, 4567–4607, 2009

Table 2. Average organic mass concentrations ($\mu g/m^3$), major functional group mass contributions PMF factors to elements with $r>0.53$ (bold) and $0.4<r<0.53$ by sampling platforms.

	3 Factors			4 Factors			5 Factors			6 Factors		
	SIMAT	Altzomoni	C130	SIMAT	Altzomoni	C130	SIMAT	Altzomoni	C130	SIMAT	Altzomoni	C130
Factor 1 (combustion I)		Fe, Ni, Br			Mn, Br			**Br**, Mn, Fe			Mn, Fe, Zn, Br	
	1.2	0.9	0.7	0.8	0.5	0.1	0.2	0.2	0.1	0.3	0.2	0.1
Alcohol groups		7%			21%			12%			15%	
Alkane groups		48%			27%			27%			20%	
Non-acid carbonyl groups		25%			37%			0			44%	
Amine groups		16%			15%			24%			21%	
Carboxylic acid groups		5%			0			37%			0	
O/C		0.3			0.6			0.6			0.6	
Factor 2 (mixed or processed)		–			Ca			–			–	
	1.9	2.2	0.7	1.9	2.3	0.6	0.9	1.7	0.8	1.0	1.7	0.7
Alcohol groups		47%			43%			67%			68%	
Alkane groups		22%			23%			13%			12%	
Amine groups		8%			10%			11%			11%	
Carboxylic acid groups		7%			9%			9%			9%	
O/C		0.8			0.8			1.2			1.2	
Factor 3 (combustion II)	**S**, K, Ca, Mn, Fe, Cu, Zn, Br			**S**, Se, K, Mn, Fe, Br			**S**, Se K, Mn, Fe, Zn			**S**, Se, Zn		
	6.6	4.7	4.6	3.6	2.3	2.2	3.5	2.1	2.0	2.8	1.5	2.0
Alcohol groups		11%			11%			17%			16%	
Alkane groups		54%			61%			62%			65%	
Amine groups		6%			2%			0%			0%	
Carboxylic acid groups		29%			26%			21%			19%	
O/C		0.4			0.3			0.3			0.3	
Factor 4 (combustion III)		–			**Br**, S			**Br**, S			**Br, S**, K	
	–	–	–	3.6	2.9	3.3	3.8	3.4	3.7	4.5	4.1	2.1
Alcohol groups		–			7%			12%			15%	
Alkane groups		–			51%			47%			48%	
Amine groups		–			12%			9%			8%	
Carboxylic acid groups		–			30%			32%			29%	
O/C		–			0.4			0.4			0.4	
Factor 5 (biomass burning)		–			-		**K, Mn, Fe, Br**, S, Cl, Ca, Cu, Pb			**K, Mn, Fe, Br**, S, Cl, Ca, Cu, Pb		
	–	–	–	–	–	–	3.0	1.4	0.6	3.2	1.5	0.5
Alcohol groups		–			–			22%			27%	
Alkane groups		–			–			33%			32%	
Non-acid carbonyl groups		–			–			36%			34%	
Amine groups		–			–			8%			8%	
O/C		–			–			0.5			0.6	
Factor 6 (C130)		–			–			–			**Ni**, Ba, Hg	
	–	–	–	–	–	–	–	–	–	0	0	1.0
Alcohol groups		–			–			–			15%	
Alkane groups		–			–			–			61%	
Carboxylic acid groups		–			–			–			20%	
O/C		–			–			–			0.3	

ACPD
9, 4567–4607, 2009

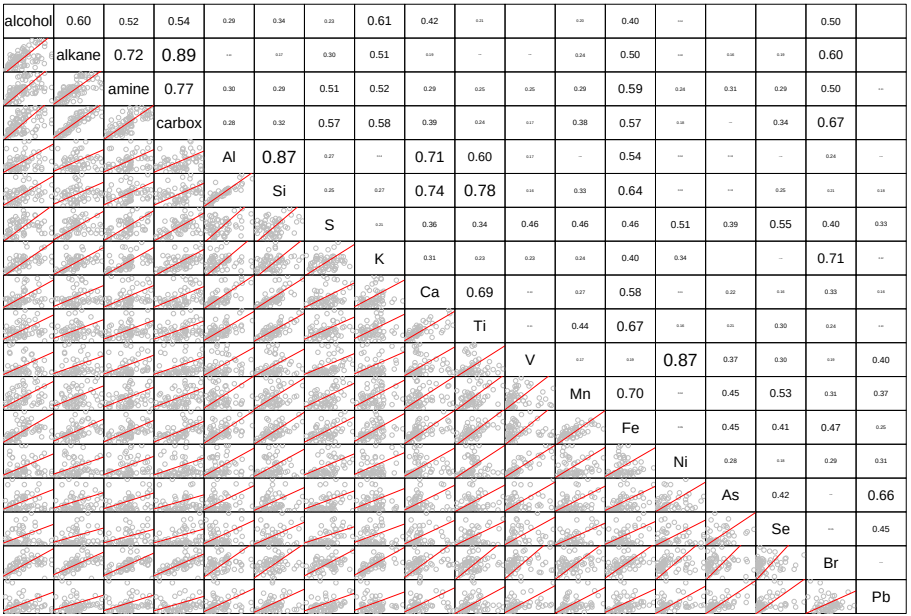

Fig. 1a. Scatter plots (lower left panels) and correlation coefficients of FTIR organic functional group and XRF elemental concentrations for **(a)** SIMAT, **(b)** Altzomoni, and **(c)** C130 platforms. Font size of correlation coefficients is scaled by its value to highlight the strongest correlations. Best fit lines are included where $r>0.5$.

ACPD
9, 4567–4607, 2009

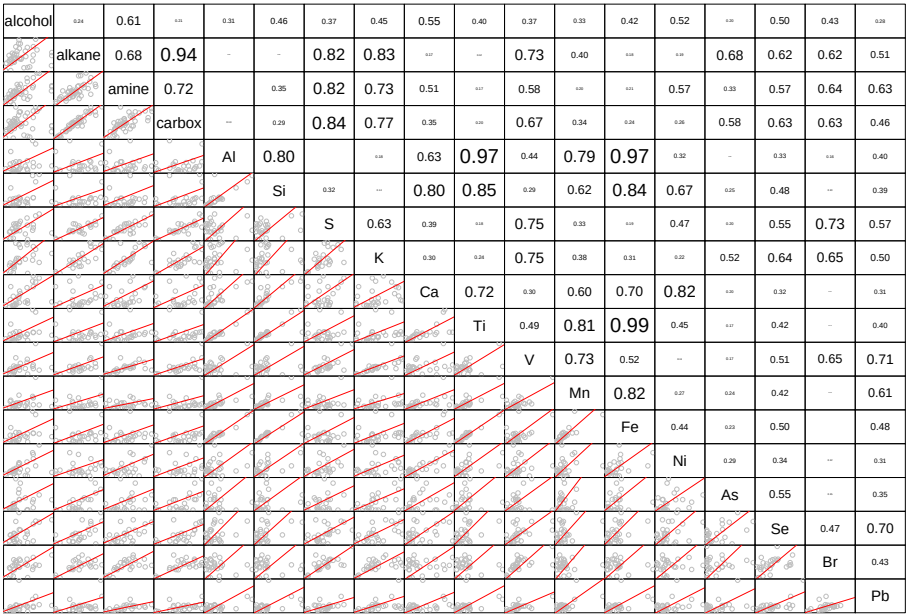

Fig. 1b. Continued.

ACPD
9, 4567–4607, 2009

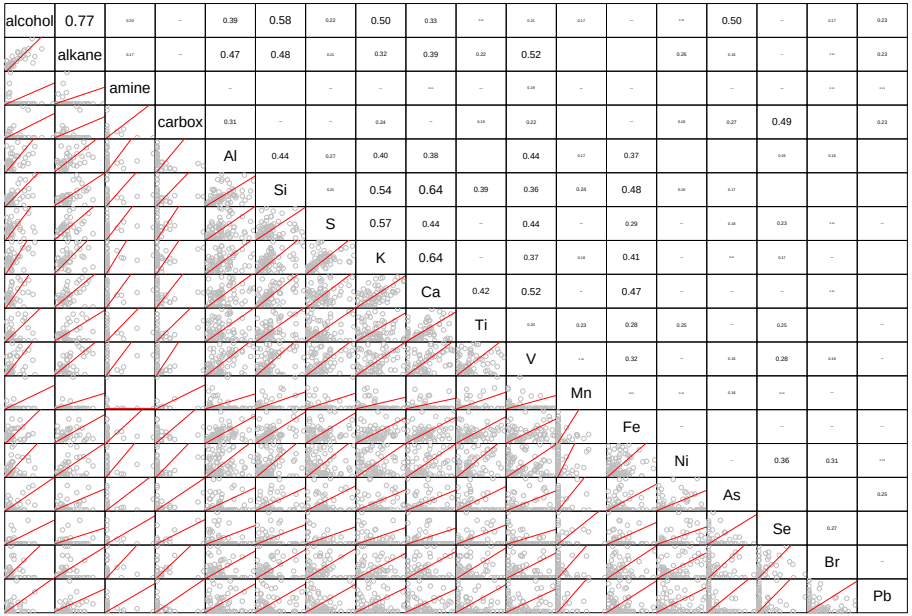

Fig. 1c. Continued.

ACPD
9, 4567–4607, 2009

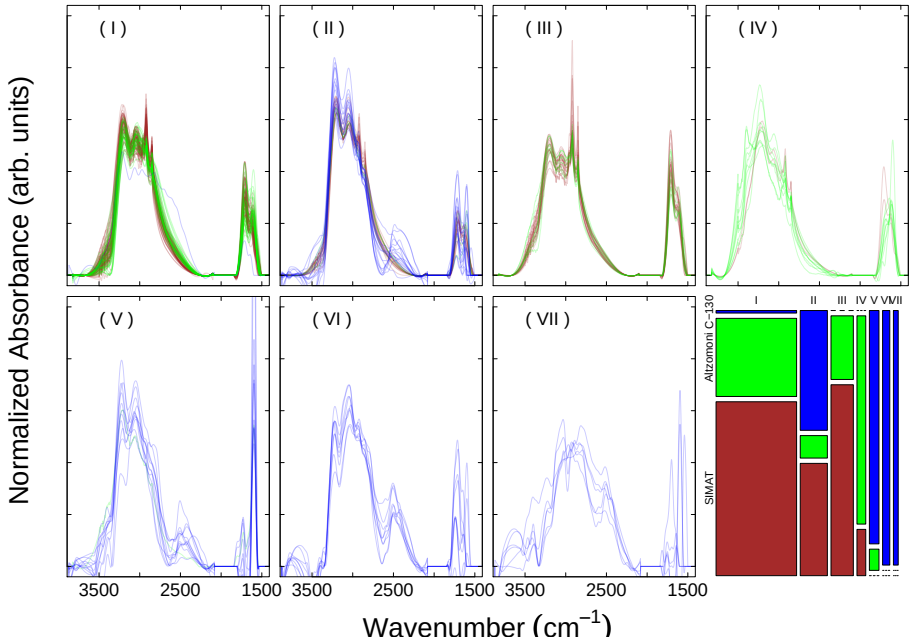

Fig. 2. FTIR spectra during MILAGRO 2006 from cluster categories I–VII (panels I–VII) and cluster-platform comparison plot (the last panel) showing the number of samples associated with each cluster for each platform. Colors indicate SIMAT (brown), Altzomoni (green), and C130 (blue).

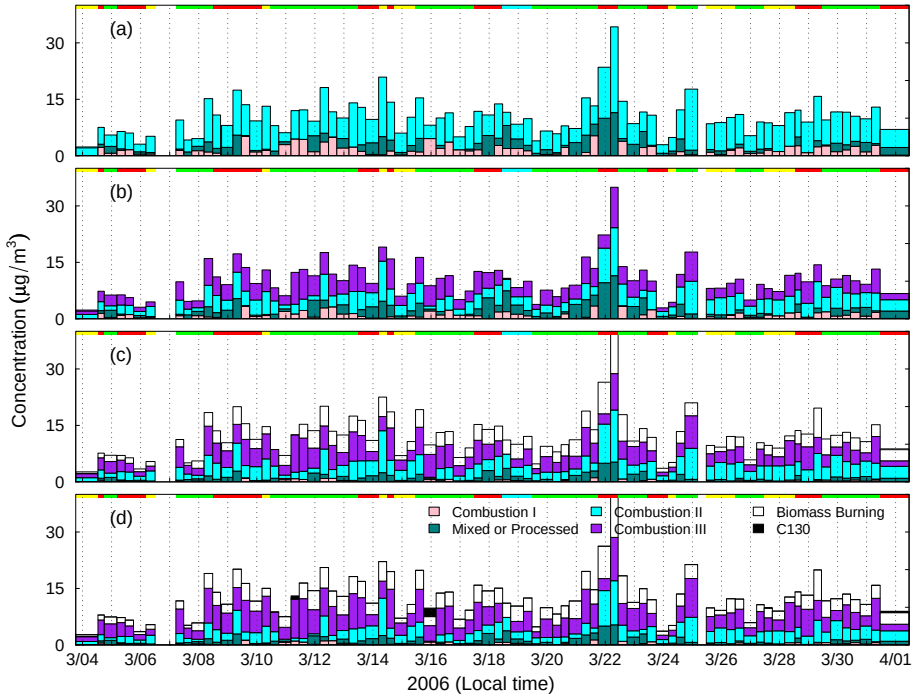

Fig. 3a. OM factor concentrations for combustion I (pink), mixed or processed (teal), combustion II (cyan), combustion III (purple), biomass burning (white), and C130 (black) factors for (i) 3, (ii) 4, (iii) 5, and (iv) 6-factor PMF of FTIR spectra with cluster I (red), cluster II (yellow), cluster III (green), cluster IV (cyan), cluster V (blue), cluster VI (purple), and cluster VII (pink) marked by top colored bars for SIMAT (panel 1), Altzomoni (panel 2), and C130 (panel 3) platforms.

ACPD
9, 4567–4607, 2009

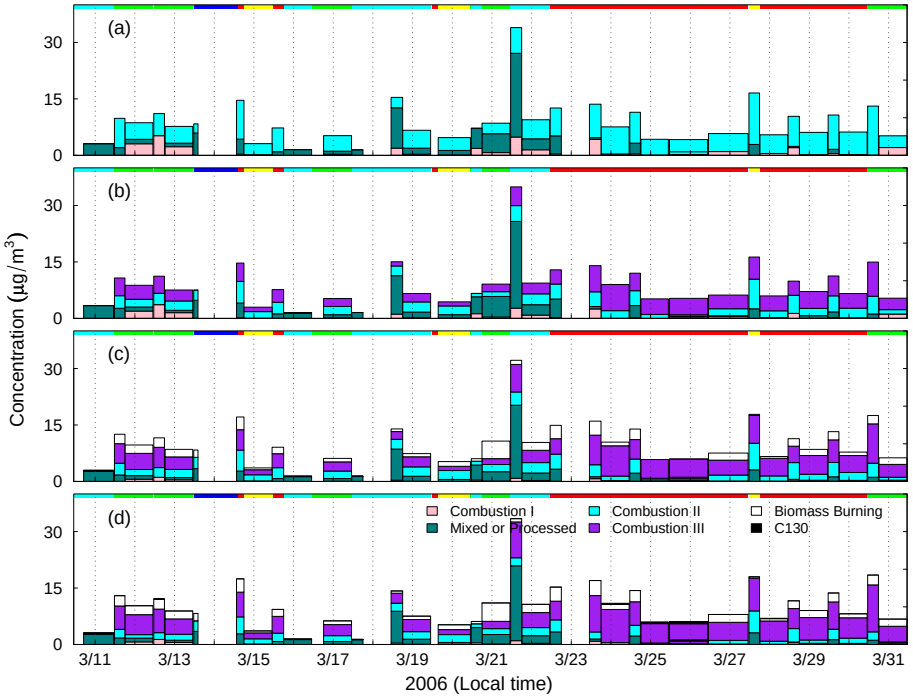

Fig. 3b. Continued.

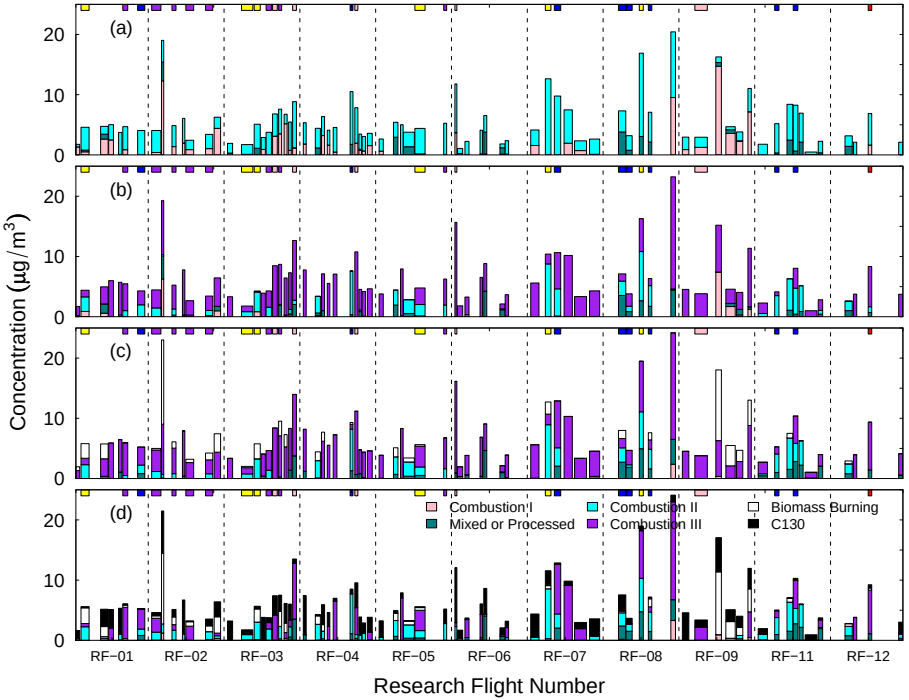

Fig. 3c. Continued.

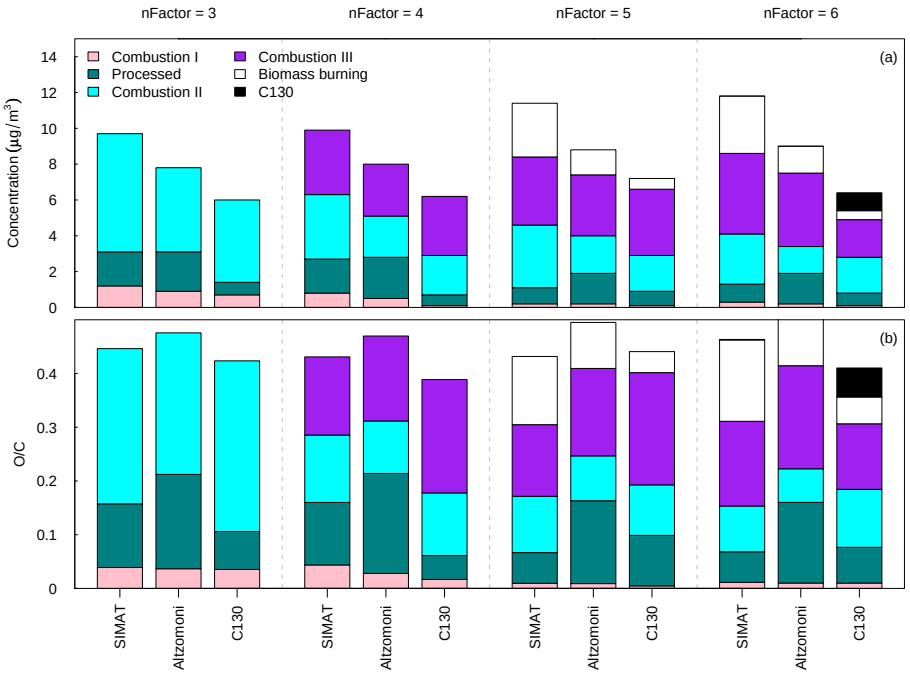

Fig. 4. Average contributions of OM concentrations **(a)** and O/C **(b)** of combustion I (pink), mixed or processed (teal), combustion II (cyan), combustion III (purple), biomass burning (white), and C130 (black) factors for 3, 4, 5, and 6-factor FTIR PMF runs.

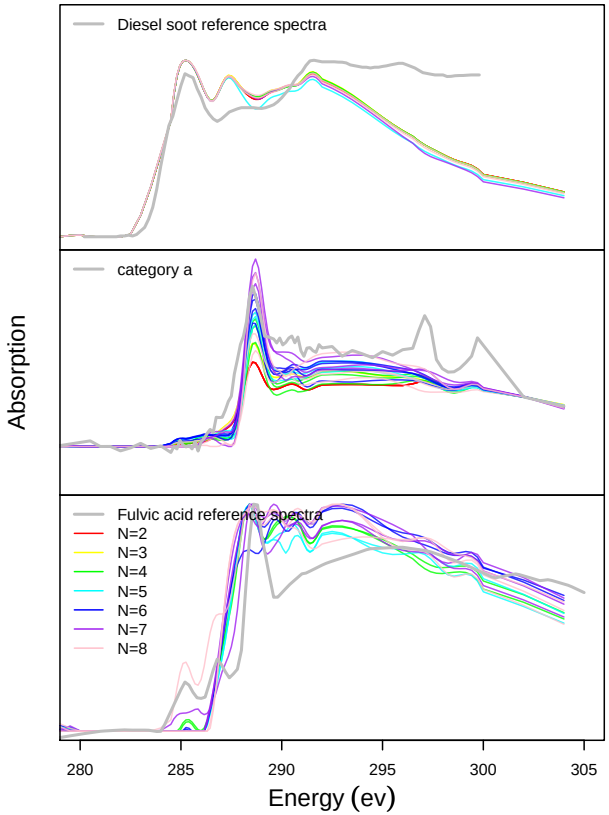

Fig. 5. Comparisons of major factor spectra from PMF of NEXAFS-STXM spectra with reference spectra: diesel soot (Braun, 2005), category a (Takahama et al., 2007), and fulvic acid (Ade and Urquhart, 2002). Colors indicate 2 (red), 3 (yellow), 4 (green), 5 (cyan), 6 (blue), 7 (purple), and 8-factor (pink) PMF run.

ACPD
9, 4567–4607, 2009

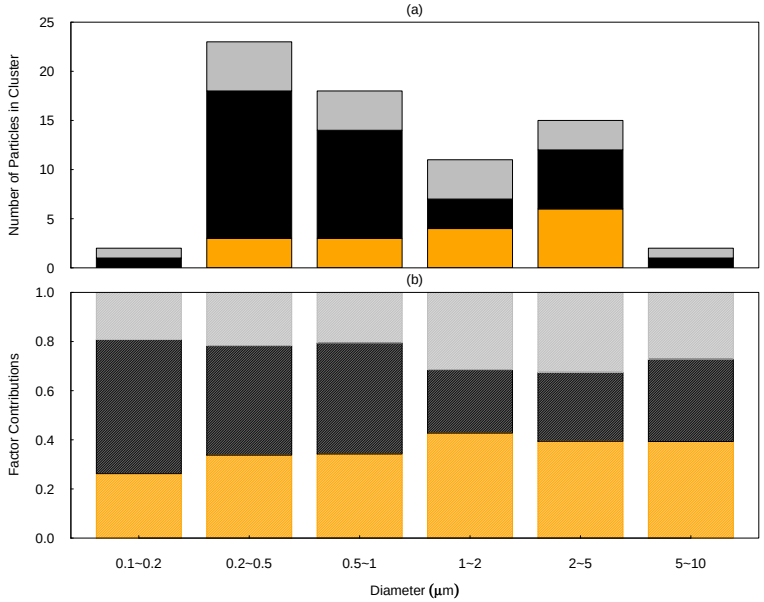

Fig. 6. (a) size distributions of NEXAFS-STXM analyses for "secondary" type – corresponding to category (a), "soot" type – corresponding to categories (b), (c), (d), (d), (e), (g), (h), and (m), and "biomass burning" type (corresponding to categories (i) and (j)) particles described by Takahama et al. (2007). Colors indicate NEXAFS-STXM cluster categories for "secondary" (orange), "soot" (black), and "biomass burning" (grey). **(b)** average fractions of processed (orange), soot (black), and biomass burning (grey) factors in 0.1–0.2 μm, 0.2–0.5 μm, 0.5–1 μm, 1–2 μm, 2–5 μm, and 5–10 μm size ranges for 4-factor PMF run of NEXAFS-STXM spectra.

ACPD
9, 4567–4607, 2009

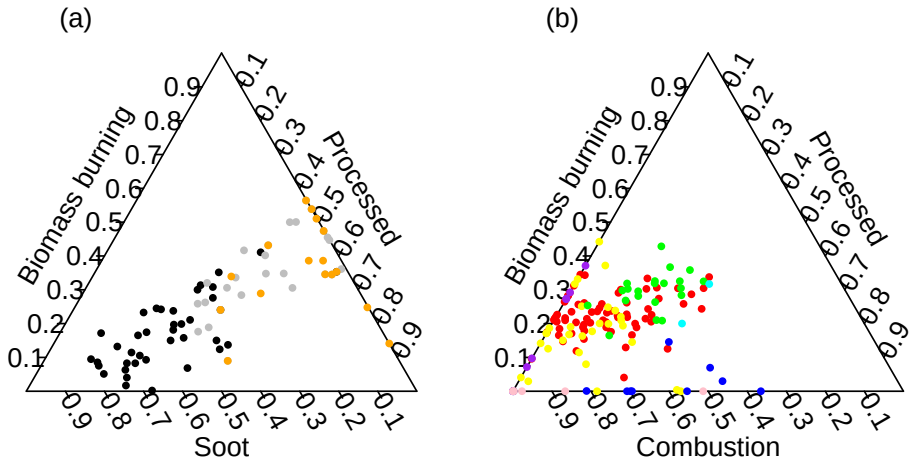

Fig. 7. (a): ternary plot of soot, processed, and biomass burning factor fractions from PMF of NEXAFS-STXM spectra. Colors indicate clusters associated with soot type (b-e, g, h, m) particles (black), processed type (a) particles (orange), and biomass burning type (i, j) particles (grey). **(b)**: ternary plot of combustion, processed, and biomass burning factor fractions from 6-factor PMF of FTIR spectra. Colors indicate cluster I (red), cluster II (yellow), cluster III (green), cluster IV (cyan), cluster V (blue), cluster VI (purple), and cluster VII (pink).

ACPD
9, 4567–4607, 2009

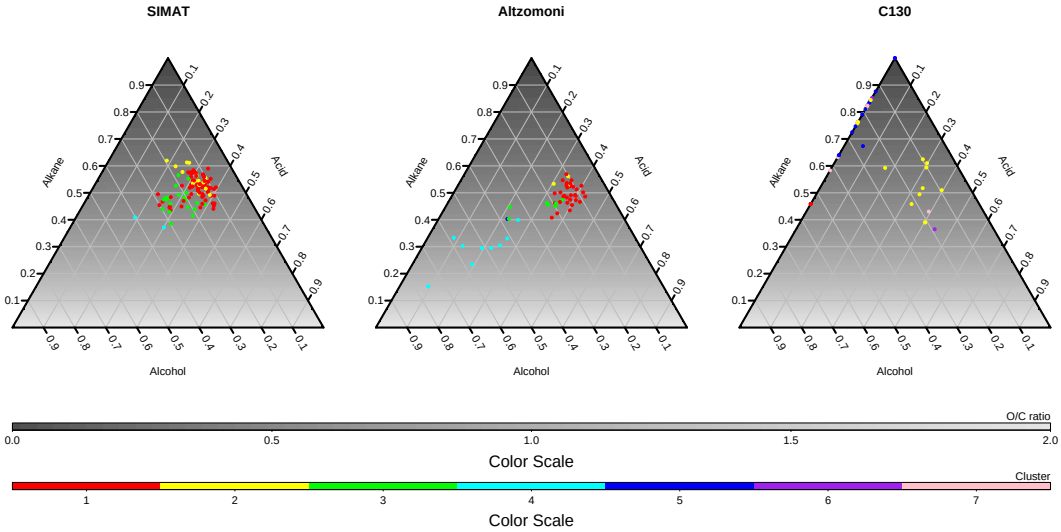

Fig. 8. Ternary plot of alcohol, alkane, and carboxylic acid functional group mass fractions of SIMAT, Altzomoni, and C130 FTIR measurements. Surface shading indicates O/C. Colors of cluster groups for FTIR spectra indicate cluster I (red), cluster II (yellow), cluster III (green), cluster IV (cyan), cluster V (blue), cluster VI (purple), and cluster VII (pink).

ACPD
9, 4567–4607, 2009